

## Section 2

# ADVANCED TECHNOLOGY DEVELOPMENTS

### 2.A Fokker-Planck Modeling of Electron Transport

Just over a decade ago Bell *et al.*<sup>1</sup> produced one of the first Fokker-Planck (FP) simulations of electron-energy transport in an idealized laser-produced plasma. As a result of improvements in numerical techniques and computational speeds available from modern computers, it is now possible to routinely run FP codes under conditions directly relevant to inertial confinement fusion (ICF).<sup>2-5</sup> The relevance of such simulations is that ICF plasmas can exhibit conditions where classical fluid transport theory<sup>6,7</sup> is inadequate.

Well-known manifestations of the breakdown of fluid theory occur in the presence of strong temperature gradients, where the Spitzer-Härm (SH) heat flow  $\mathbf{q}_{SH} = -\kappa_{SH} \nabla T$  ( $\kappa_{SH}$  being the SH thermal conductivity and  $T$  the electron temperature) overestimates the magnitude of the maximum heat flux and fails to predict the preheat caused by long-mean-free-path electrons ahead of the main heat front.<sup>1</sup> Although the first inadequacy can be overcome to some extent by limiting the heat flow to some fraction  $f$  of its “free-streaming” limit  $q_f$ ,<sup>8</sup> i.e.,  $\mathbf{q} = \mathbf{q}_{SH} / (1 + |\mathbf{q}_{SH}| / f q_f)$ , the second one can only be properly corrected by means of a nonlocal heat-transport model such as the FP equation.

A more subtle heat-flow reduction effect has also been shown to arise<sup>9</sup> even for arbitrarily small levels of heat flow (i.e.,  $|\mathbf{q}_{SH}| \ll f q_f$ ), provided that the characteristic wavelength of the temperature modulation is less than about  $200 \lambda_e$ , where  $\lambda_e$  is the delocalization length or mean free path of a thermal electron.<sup>3,10,11</sup> This phenomenon has been shown to have important consequences for laser filamentation instabilities,<sup>10</sup> as confirmed by recent simulations of experiments,<sup>4,12</sup> and to stimulated Brillouin scattering.<sup>13-15</sup>

This article addresses some of the computational issues involved in solving the FP equation. Particular emphasis will be given to the development of codes applicable to laser-fusion problems of the type previously mentioned. The FP equation is first introduced; the two-dimensional (2-D) electron FP code (*SPARK*) is described; this is followed by numerical simulations and a discussion of future directions.

### The Fokker-Planck Equation

The Fokker-Planck equation for Coulomb collisions between species  $a$  and  $b$  with respective distribution functions  $f_a(\mathbf{r}, \mathbf{v}, t)$  and  $f_b(\mathbf{r}, \mathbf{v}, t)$  can be written as<sup>16</sup>

$$\begin{aligned} \frac{\partial f_a}{\partial t} + \mathbf{v} \cdot \nabla f_a + \frac{Z_a e}{m_a} \mathbf{E} \cdot \nabla_{\mathbf{v}} f_a \\ = Y_{ab} \left[ -\nabla_{\mathbf{v}} \cdot (f_a \nabla_{\mathbf{v}} H_{ab}) + \frac{1}{2} \nabla_{\mathbf{v}} \nabla_{\mathbf{v}} : (f_a \nabla_{\mathbf{v}} \nabla_{\mathbf{v}} G_{ab}) \right], \quad (1) \\ + Y_{aa} \left[ -\nabla_{\mathbf{v}} \cdot (f_a \nabla_{\mathbf{v}} H_{aa}) + \frac{1}{2} \nabla_{\mathbf{v}} \nabla_{\mathbf{v}} : (f_a \nabla_{\mathbf{v}} \nabla_{\mathbf{v}} G_{aa}) \right], \end{aligned}$$

where

$$Y_{ab} = 4\pi \left( \frac{Z_a Z_b e^2}{m_a} \right)^2 \ln \Lambda, \quad (2)$$

$$H_{ab}(\mathbf{v}) = \frac{m_a + m_b}{m_b} \int \frac{f_b(\mathbf{v}')}{|\mathbf{v} - \mathbf{v}'|} d\mathbf{v}', \quad (3a)$$

and

$$G_{ab}(\mathbf{v}) = \int f_b(\mathbf{v}') |\mathbf{v} - \mathbf{v}'| d\mathbf{v}', \quad (3b)$$

where  $\nabla$  is the configuration space gradient operator,  $\nabla_{\mathbf{v}}$  is the velocity space gradient operator,  $\ln \Lambda$  is the Coulomb logarithm (for simplicity assumed to be the same for both particles),  $e$  is magnitude of the electronic charge,  $Z_a$  and  $Z_b$  are the respective charge numbers of particles  $a$  and  $b$ , and  $m_a$  and  $m_b$  are their respective masses. The left-hand side of Eq. (1) (usually known as the Vlasov part) represents the collisionless transport of particle  $a$  in the presence of an accelerating field  $Z_a e \mathbf{E} / m_a$ , but in the absence of magnetic field effects. The collisional term on the right-hand side of Eq. (1) assumes the dominance of small-angle scattering, which implies that  $\ln \Lambda \gg 1$ .

### The *SPARK* Code

The basic philosophy behind the *SPARK* code has been to provide an efficient and robust way of solving the FP equation.<sup>17,18</sup> Its main purpose has been to study nonlocal heat-transport problems of interest to ICF.

*SPARK* is not unlike a standard hydrodynamic code, in that it solves the fluid equation for the ions (mass and momentum conservation) and the energy equation for the electrons (neglecting ion-thermal effects). However, the latter is modeled by the FP equation instead of a fluid equation with SH heat flow.

Current versions of the code neglect the effects of magnetic fields and allow for one-dimensional (1-D) Lagrangian transport in planar, cylindrical, or spherical geometry, and 2-D Eulerian transport in either planar or cylindrical geometry. The 2-D version incorporates a paraxial wave-equation approach for laser light transport.<sup>12</sup> In all versions, the fluid-transport equations (with SH electron heat flow) are solved in parallel so as to assess the importance of kinetic effects and provide for an accuracy check of the FP code in the collisional limit.

### 1. Basic Equations

The electron FP equation solved in *SPARK* includes an inverse-bremsstrahlung heating source.<sup>19</sup> By defining the distribution function in the reference frame of the fluid ions (of velocity  $\mathbf{u}_i$ ), and using the expansion  $f = f_0 + \mathbf{v} \cdot \mathbf{f}_1 / v$ , Eq. (1) becomes

$$\begin{aligned}
 & \left( \frac{\partial}{\partial t} + \mathbf{u}_i \cdot \nabla \right) f_0 - (\nabla \cdot \mathbf{u}_i) \frac{v}{3} \frac{\partial f_0}{\partial v} = \nabla \cdot \left[ \chi (\nabla f_0 + \mathbf{a} \alpha f_0) \right] \\
 & \hspace{10em} (a) \hspace{10em} (b) \\
 & + \frac{1}{v^2} \frac{\partial}{\partial v} \left[ \chi \left( \mathbf{a} \cdot \mathbf{a} \frac{\partial f_0}{\partial v} + v \boldsymbol{\beta} \cdot \mathbf{a} f_0 \right) + Y_{ee} \left( C_0 f_0 + D_0 \frac{\partial f_0}{\partial v} \right) \right] \\
 & \hspace{10em} (c) \hspace{10em} (d) \\
 & + \left. \frac{n_e Z^* Y_{ee} v_0^2}{6v} \frac{\partial f_0}{\partial v} + \frac{H_{\text{vis}}}{v} \frac{\partial f_0}{\partial v} \right], \hspace{10em} (4) \\
 & \hspace{10em} (e) \hspace{10em} (f)
 \end{aligned}$$

where  $v_0$  is the electron oscillatory velocity in the laser field,  $\mathbf{a} = e\mathbf{E}/m_e$ ,  $\alpha = -(\partial_v \ln f_0)/v$ ,  $\boldsymbol{\beta} = -\nabla \ln f_0$ , and  $\chi = v^2/3v_{ei}^*$ . Here, we have introduced an effective  $e$ - $i$  collision frequency defined by  $v_{ei}^* = \phi 4\pi n_e Z^* (e^2/m_e)^2 \ln \Lambda / v^3$ , where  $Z^* = \langle Z^2 \rangle / \langle Z \rangle$  (with  $\langle \rangle$  denoting an average of the ion species), and  $\phi = (Z^* + 4.2)/(Z^* + 0.24)$  is a factor that gives rise to the ‘‘exact’’ SH heat flow (for arbitrary  $Z$  when  $f_0$  is a Maxwellian).<sup>3,20</sup> The terms in Eq. (4) can be identified as (a) hydrodynamic advection and compression, (b) electron transport in configuration space, (c) ohmic heating, (d)  $e$ - $e$  thermalization, (e) laser heating, and (f) heating caused by ion viscosity. The computational strategy for dealing with these various terms will be discussed.

Two important moments of Eq. (4) are the particle density moment  $\left( 4\pi \int dv v^2 \right)$

$$\left( \frac{\partial}{\partial t} + \mathbf{u}_i \cdot \nabla \right) n_e + n_e \nabla \cdot \mathbf{u}_i = 0, \hspace{10em} (5)$$

and the energy-density moment  $\left(2\pi m_e \int dvv^4\right)$

$$\left(\frac{\partial}{\partial t} + \mathbf{u}_i \cdot \nabla\right) \frac{3}{2} p + \frac{5}{2} p \nabla \cdot \mathbf{u}_i = -\nabla \cdot \mathbf{q} + s_{\text{ib}} + h_{\text{vis}} , \quad (6)$$

where  $n_e = 4\pi \int dvv^2 f_0$  is the electron number density,  $p = (4\pi/3) \int dvv^4 f_0$  is the electron pressure, and  $s_{\text{ib}}$  and  $h_{\text{vis}}$  are the respective inverse-bremsstrahlung and viscous heating. In deriving Eqs. (5) and (6) we have enforced quasi-neutrality by imposing zero current in the plasma. This condition allows us to calculate the electric field as follows:

$$\mathbf{a} = -\frac{\int dvv^2 \chi \nabla f_0}{\int dvv^2 \chi \alpha f_0} = -\frac{\int dvv^2 \chi \mathbf{B} f_0}{\int dvv \chi \frac{\partial f_0}{\partial v}} . \quad (7)$$

An alternative approach for calculating the electric field would be to adopt the implicit-moment method,<sup>21</sup> where one would use charge conservation and the Poisson equation to solve for  $\mathbf{E} = -\nabla \Phi$ . Although this method has been found to improve charge neutrality in FP calculations, it has only a negligible effect on the thermal transport results.<sup>17</sup>

Conservation of ion density and total momentum (assuming cold ions) is given by

$$\left(\frac{\partial}{\partial t} + \mathbf{u}_i \cdot \nabla\right) n_i + n_i \nabla \cdot \mathbf{u}_i = 0 \quad (8)$$

and

$$m_i n_i \left(\frac{\partial}{\partial t} + \mathbf{u}_i \cdot \nabla\right) \mathbf{u}_i = -\nabla(p + Q_{\text{vis}}) + \mathbf{P}_F , \quad (9)$$

respectively, where  $\mathbf{P}_F$  is the ponderomotive force and  $Q_{\text{vis}}$  is the artificial viscosity.<sup>22</sup>

## 2. The Alternating-Direction-Implicit (ADI) Method of Solution

The aim of the ADI method is to provide a time-implicit solution of a multidimensional differential equation by splitting it into 1-D equations,<sup>23,24</sup> which can then be efficiently solved. For a differential equation of the type

$$\frac{\partial f_0}{\partial t} = (F_x + F_y + F_v) f_0 , \quad (10)$$

where  $F_x$ ,  $F_y$ , and  $F_v$  are operators in  $x$ ,  $y$ , and  $v$ , the scheme becomes

$$(1 - \theta \Delta t F_x) (f_0^* - f_0^n) = \Delta t (F_x + F_y + F_v) f_0^n , \quad (11a)$$

$$(1 - \theta \Delta t F_y)(f_o^{**} - f_o^n) = (f_o^* - f_o^n), \quad (11b)$$

and

$$(1 - \theta \Delta t F_v)(f_o^{n+1} - f_o^n) = (f_o^{**} - f_o^n). \quad (11c)$$

Here we have differenced in time as  $\partial f / \partial t = (f^{n+1} - f^n) / \Delta t$  and introduced the implicitness parameter  $\theta$ , such that Eqs. (11a)–(11c) combined become accurate to  $O(\Delta t)^2$ , when  $\theta = 1/2$  (like the Crank-Nicolson scheme).

To put the FPEq. (4) into the form of Eq. (10), we first assume (without loss of generality) that the distribution  $f_o$  is a function of  $x$ ,  $y$ , and  $v$  and neglect the hydrodynamic contribution [term (a) in Eq. (4)]. Since the hydrodynamics usually evolves on a much longer time scale than the electron thermal transport, its contribution can be treated separately.

Next, we assume that operators  $F_x(f_o)$ ,  $F_y(f_o)$ , and  $F_v(f_o)$  are weak functions of  $f_o$ . To deal with the nonlinearities we may choose to (a) iterate at each time step by starting with  $F^n = F(f_o^n)$ ; (b) use a predictor step

$$F = F\left[f_o^n + \theta(f_o^n - f_o^{n-1})\right], \quad (12)$$

followed by iteration;<sup>17</sup> or (c) linearize the operator as follows:<sup>25</sup>

$$F^{n+1} = F^n + \left(\frac{\partial F}{\partial f_o}\right)^n (f_o^{n+1} - f_o^n) + O(\Delta t)^2. \quad (13)$$

The choice between these various options becomes particularly important when dealing with the  $e$ - $e$  thermalization [term (d), Eq. (4)], as will be discussed.

The remaining problem with Eq. (4) lies in the  $E$ -field terms. Not only are they nonlinear [see Eq. (7)], but they also involve mixed derivatives like  $\partial_x \partial_v f_o$ ,  $\partial_y \partial_v f_o$ , ... that cannot easily be incorporated into the ADI scheme. A way around this difficulty has been found by introducing the coefficients  $\alpha(f_o)$  and  $\beta(f_o)$  in Eq. (4), which are then treated as time invariant over a time step  $\Delta t$ .<sup>26</sup> With this transformation the FPEquation can be expressed in the form of Eq. (10), where  $F_x$ ,  $F_y$ , and  $F_v$  are convection-diffusion operators.

To difference Eq. (4) (in the 2-D Eulerian version of *SPARK*), the distribution function is defined on an orthogonal grid  $f_{j,k,l} = f_o(v_j, x_k, y_l)$ , where the indices  $j = 1, \dots, J$ ,  $k = 1, \dots, K$ , and  $l = 1, \dots, L$ , denote cell centers. The cell boundaries are defined by  $v_{j+1/2} = (v_j + v_{j+1})/2, \dots$ , and the cell sizes (not necessarily uniform) by  $\Delta v_j = (v_{j+1/2} - v_{j-1/2}), \dots$ . In the 1-D Lagrangian version, a mesh-centered grid is used in configuration space.<sup>27</sup>

### 3. Hydrodynamic Transport

Since the hydrodynamic evolution of the plasma is normally slow compared with the thermal-transport processes, we are able to solve the left-hand side of Eq. (4) separately. In the 2-D Eulerian version of *SPARK* we adopt a standard

donor-cell scheme<sup>22</sup> for the convective terms in Eqs. (4), (8), and (9) and set  $Q_{\text{vis}} = 0$ . (However, if one wishes to model sharp density gradients and shocks, a less-diffusive numerical scheme would be desirable.)

In the 1-D Lagrangian version, the fluid equations (8) and (9) are solved in the frame of the ions, by introducing the total derivative  $d/dt = (\partial/\partial t + \mathbf{u}_i \cdot \nabla)$ .<sup>22</sup> The left-hand side of Eq. (4) is solved in the form<sup>3</sup>

$$\frac{f_o^{n+1} - f_o^n}{\Delta t} + \frac{d(\ln n_i)}{dt} \left[ \frac{v}{3} \frac{\partial (\ln f_o^n)}{\partial v} \right] f_o^n = 0, \quad (14)$$

where we have made use of the continuity equation  $\nabla \cdot \mathbf{u}_i = -d(\ln n_i)/dt$ .

In both Eulerian and Lagrangian versions of the code the transformation  $\partial_v f_o = f_o \partial_v \ln f_o$  has been used, where  $[\partial_v \ln f_o]_j \approx [\ln(f_{j+1}/f_{j-1})]/2\Delta v_j$ . This formulation gives rise to zero truncation error for a Maxwellian and has been found to minimize departures from quasi-neutrality.

#### 4. Electron Transport in Configuration Space

The electron transport in configuration space [term (b) in Eq. (4)] is differenced in conservative form as follows:

$$\begin{aligned} & \nabla \cdot [\chi(\nabla f_o + \mathbf{a}\alpha f_o)]_{j,k,l} \\ &= \frac{1}{\Delta x_k} \left[ \chi_{k+1/2} \left( \frac{f_{k+1} - f_k}{\Delta x_{k+1/2}} + a_{x,k+1/2} \alpha_{k+1/2} f_{k+1/2} \right) \right. \\ & \quad \left. - \chi_{k-1/2} \left( \frac{f_k - f_{k-1}}{\Delta x_{k-1/2}} + a_{x,k-1/2} \alpha_{k-1/2} f_{k-1/2} \right) \right]_{j,l} \\ & \quad + \frac{1}{\Delta y_l} \left[ \chi_{l+1/2} \left( \frac{f_{l+1} - f_l}{\Delta y_{l+1/2}} + a_{y,l+1/2} \alpha_{l+1/2} f_{l+1/2} \right) \right. \\ & \quad \left. - \chi_{l-1/2} \left( \frac{f_l - f_{l-1}}{\Delta y_{l-1/2}} + a_{y,l-1/2} \alpha_{l-1/2} f_{l-1/2} \right) \right]_{j,k}. \end{aligned} \quad (15)$$

Here, the boundary values of  $f$  are calculated using an interpolation formula of type

$$f_{j,k+1/2,l} = (1 - \epsilon_{j,k+1/2,l}) f_{j,k+1,l} + \epsilon_{j,k+1/2,l} f_{j,k,l}, \quad (16)$$

(and similarly for  $f_{j,k,l+1/2}$ ), where

$$\varepsilon_{j,k+1/2,l} = \left[ 1 - \text{sign}(a_{x,k+1/2,l} \alpha_{x,k+1/2,l}) \right] / 2$$

ensures up-wind differencing for the convection term  $\nabla \cdot (\mathbf{a} \alpha f_0)$ .

The respective values of  $a_{x,k+1/2,l}$  and  $a_{x,k+1/2,l}$  are obtained from

$$a_{x,k+1/2,l} = - \frac{\sum_{j=1}^J \Delta v_j v_j^2 \chi_{j,k+1/2,l} (f_{k+1} - f_k)_{j,l} / \Delta x_{k+1/2}}{\sum_{j=1}^J \Delta v_j v_j^2 \chi_{j,k+1/2,l} \alpha_{j,k+1/2,l} f_{j,k+1/2,l}} \quad (17)$$

[using Eq. (7)] and

$$\alpha_{j,k+1/2,l} = - \frac{1}{2v_j \Delta v_j} \ln \left( \frac{f_{j+1}}{f_{j-1}} \right)_{k+1/2,l}. \quad (18)$$

### 5. $e$ - $e$ Thermalization

In the absence of thermal transport and external heating, the usual time-implicit difference version of Eq. (4) is<sup>28</sup>

$$\begin{aligned} \frac{f_j^{n+1} - f_j^n}{\Delta t} = & \frac{Y_{ee}}{\Delta v_j v_j^2} \left[ C_{j+1/2} f_{j+1/2}^{n+1} - C_{j-1/2} f_{j-1/2}^{n+1} \right. \\ & \left. + \frac{D_{j+1/2}}{\Delta v_{j+1/2}} (f_{j+1}^{n+1} - f_j^{n+1}) - \frac{D_{j-1/2}}{\Delta v_{j-1/2}} (f_j^{n+1} - f_{j-1}^{n+1}) \right], \quad (19) \end{aligned}$$

which, with the appropriate boundary conditions, conserves particle numbers exactly. Following the Chang-Cooper method,<sup>28</sup> we use

$$f_{j+1/2} = (1 - \delta_{j+1/2}) f_{j+1} + \delta_{j+1/2} f_j, \quad (20)$$

where

$$\delta_{j+1/2} = \frac{1}{w_{j+1/2}} - \frac{1}{\exp(w_{j+1/2}) - 1} \quad (21)$$

and  $w_{j+1/2} = \Delta v_{j+1/2} C_{j+1/2} / D_{j+1/2}$ . This type of weighting has been designed to preserve positivity and provide the correct equilibrium solution for  $f_0$ .

In order to conserve energy, the  $\Sigma(\Delta v_j v_j^4)$  sum of the right-hand side of Eq. (19) has to vanish. Langdon<sup>29</sup> has shown, through integration by parts, that this can be achieved by calculating the collisional terms as follows:

$$C_{j+1/2} = 4\pi \sum_{i=1}^j (\Delta v v^2 f)_i, \quad (22a)$$

$$(vD)_{j+1/2} = (vD)_{j-1/2} + (\Delta v v^2)_j 4\pi \sum_{i=j}^{J-1} (vf)_{i+1/2} \Delta v_{i+1/2}, \quad (22b)$$

and

$$(vD)_{3/2} = (\Delta v v^2)_1 4\pi \sum_{i=1}^{J-1} (vf)_{i+1/2} \Delta v_{i+1/2}. \quad (22c)$$

This method of solution implicitly assumes that  $C$  and  $D$  are slowly varying functions of time, so they can be calculated iteratively over one time step. However, when the plasma is far from equilibrium and one wishes to use time steps larger than the thermalization time  $\tau_{ee}$ , energy conservation may require too many iterations. One possible solution to this problem is to use a predictor-corrector scheme, whereby one starts the iteration by linearly extrapolating the distribution function from the  $n$  and  $(n-1)$  time levels to the  $(n+1)$  level.<sup>17</sup> An alternative approach is to linearize the full collision operator [Eq. (13)], so that Eq. (19) becomes

$$\begin{aligned} \frac{f_j^{n+1} - f_j^n}{\Delta t} &= \frac{Y_{ee}}{\Delta v_j v_j^2} \left[ C_{j+1/2}^n f_{j+1/2}^{n+1} - C_{j-1/2}^n f_{j-1/2}^{n+1} \right. \\ &\quad \left. + \frac{D_{j+1/2}^n}{\Delta v_{j+1/2}} (f_{j+1}^{n+1} - f_j^{n+1}) - \frac{D_{j-1/2}^n}{\Delta v_{j-1/2}} (f_j^{n+1} - f_{j-1}^{n+1}) \right] \\ &\quad + \frac{Y_{ee}}{\Delta v_j v_j^2} \left[ C_{j+1/2}^{n+1} f_{j+1/2}^n - C_{j-1/2}^{n+1} f_{j-1/2}^n \right. \\ &\quad \left. + \frac{D_{j+1/2}^{n+1}}{\Delta v_{j+1/2}} (f_{j+1}^n - f_j^n) - \frac{D_{j-1/2}^{n+1}}{\Delta v_{j-1/2}} (f_j^n - f_{j-1}^n) \right] \\ &\quad - \frac{Y_{ee}}{\Delta v_j v_j^2} \left[ C_{j+1/2}^n f_{j+1/2}^n - C_{j-1/2}^n f_{j-1/2}^n \right. \\ &\quad \left. + \frac{D_{j+1/2}^n}{\Delta v_{j+1/2}} (f_{j+1}^n - f_j^n) - \frac{D_{j-1/2}^n}{\Delta v_{j-1/2}} (f_j^n - f_{j-1}^n) \right], \quad (19a) \end{aligned}$$

where the right-hand side of the equation is now a full matrix operator [instead of the tridiagonal matrix in Eq. (19)]. Although a tridiagonal matrix can be more efficiently inverted than a full matrix, there are circumstances when, as a result of time-step constraints, the overall computational effort can be less for Eq. (19a) than Eq. (19).

## 6. Ohmic Heating

The ohmic-heating term [term (c) in Eq. (4)] is differenced in conservative form as follows:

$$\begin{aligned}
 & \frac{1}{v^2} \frac{\partial}{\partial v} \left[ \chi \left( \mathbf{a} \cdot \mathbf{a} \frac{\partial f_0}{\partial v} + v \boldsymbol{\beta} \cdot \mathbf{a} f_0 \right) \right]_{j,k,l} \\
 &= \frac{1}{\Delta v_j v_j^2} \left\{ \chi_{j+1/2} \left[ \left( a_x^2 + a_y^2 \right) \left( \frac{f_{j+1} - f_j}{\Delta v_{j+1/2}} \right) \right. \right. \\
 & \quad \left. \left. + \left( \beta_x a_x + \beta_y a_y \right)_{j+1/2} v_{j+1/2} f_{j+1/2} \right] \right. \\
 & \quad \left. - \chi_{j-1/2} \left[ \left( a_x^2 + a_y^2 \right) \left( \frac{f_j - f_{j-1}}{\Delta v_{j-1/2}} \right) \right. \right. \\
 & \quad \left. \left. + \left( \beta_x a_x + \beta_y a_y \right)_{j-1/2} v_{j-1/2} f_{j-1/2} \right] \right\}_{k,l}, \quad (23)
 \end{aligned}$$

where the interpolation formula for  $f_{j+1/2}$ , as well as the coefficients  $\mathbf{a}$  and  $\boldsymbol{\beta}$ , are calculated as previously shown.

Although the ohmic-heating term is normally included in FP simulations,<sup>17,30,31</sup> Town and Bell<sup>32</sup> recently suggested that since its net heating contribution vanishes for a zero-current plasma, its effect on the thermal transport might be negligible. For all *SPARK* simulations considered, this hypothesis appears to be true.

## 7. Viscous Heating

The total energy density deposited in the plasma, as a result of the viscous pressure  $Q_{\text{vis}}$  [Eq. (9)], is given by  $h_{\text{vis}} = -Q_{\text{vis}} \nabla \cdot \mathbf{u}_i$ . Since the ions are assumed cold, this energy is transferred directly to the electrons [Eq. (6)]. In the FP equation, we achieve this by introducing a collision operation [term (f), Eq. (4)] with a coefficient of the form

$$H_{\text{vis}} = \frac{2h_{\text{vis}}}{\sum_{j=1}^J v_j^2 \left( \frac{f_{j+1} - f_j}{v_{j+1/2} \Delta v_{j+1/2}} - \frac{f_j - f_{j-1}}{v_{j-1/2} \Delta v_{j-1/2}} \right)}. \quad (24)$$

## Simulations

To illustrate the capabilities of *SPARK*, we consider two simulations. The first one is of the 1-D evolution of a laser-driven planar CH foil, and the second one is of the interaction of a spatially modulated laser beam on a 2-D planar CH plasma.

### 1. Laser-Driven CH Foil in 1-D Planar Geometry

The simulation considered here applies to Rayleigh-Taylor instability experiments performed at LLNL.<sup>33</sup> It models a CH foil illuminated by 527-nm laser light, with 1-ns linear rise followed by a 2-ns flat section.

For our initial conditions we assume an 18- $\mu\text{m}$ , fully ionized CH plasma at a temperature of 0.5 eV. The peak laser intensity is chosen to be  $5 \times 10^{13} \text{ W/cm}^2$ . *SPARK* is run in 1-D planar geometry, on a Lagrangian mesh, with the full linearized version of the  $e$ - $e$  collision operator [Eq. (19a)]. The configuration space mesh uses 150 zones, and the velocity mesh uses 35 feathered zones, with  $\Delta v_{j+1} / \Delta v_j = 1.11$  and  $v_j = 266 v_t$  (where  $v_t$  is the initial thermal velocity of the electrons).

Figure 54.1 shows the (a) temperature and (b) density profiles (solid curves) near the ablation front, 2 ns after the start of the laser pulse. The laser is incident from the right, and  $z = 0$  corresponds to the initial position of the target's rear surface. Using a fixed  $\Delta t = 0.5$  ps, the run took 15 min in CPU time on a CRAY Y-MP with an overall energy-conservation error of 1%.

For comparison, Fig. 54.1 also plots (dashed curves) the results based on the fluid-electron equation with SH heat flow [Eq. (6)]. From the temperature curves we note that the fluid model predicts excessive penetration of the main heat front, yet fails to predict the preheat at the rear of the target. This preheat, which is caused by long-mean-free-path electrons coming from the 1.5-keV corona, then has the effect of decompressing the target, as seen by the broader density profile in Fig. 54.1(b).

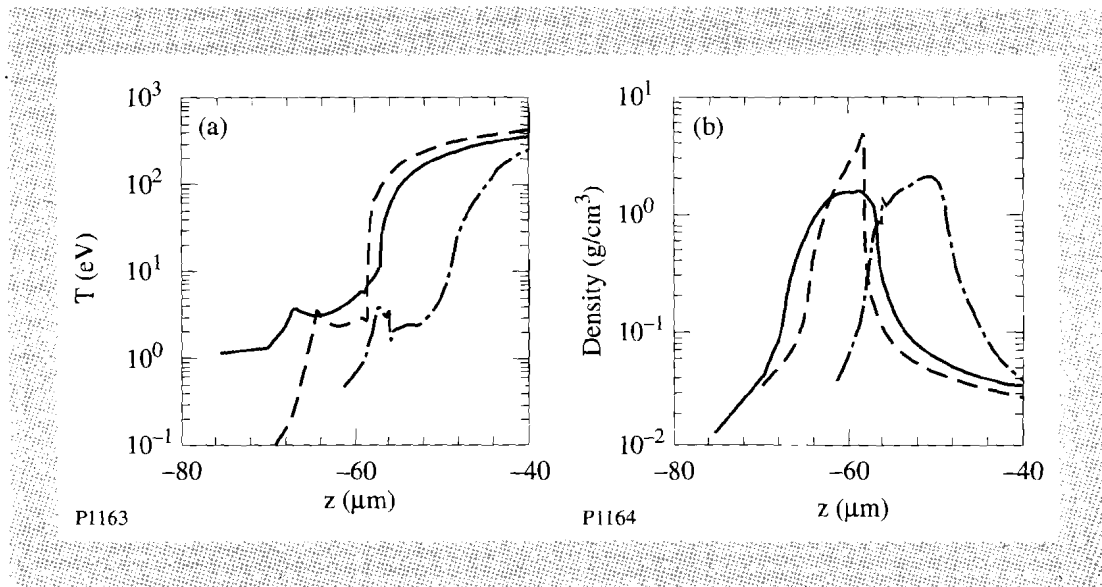


Fig. 54.1

Plots of (a) temperature in eV and (b) density in  $\text{g cm}^{-3}$  as functions of spatial position  $z$  ( $\mu\text{m}$ ) relative to the initial target surface. Solid curves correspond to FP simulation, dashed curves to SH simulation (with ideal gas equation of state, full ionization, and no radiation transport), and dash-dotted curves to *LILAC* simulation (with real equation of state, self-consistent ionization, and radiation transport).

Since the target's acceleration is found to be unaffected by the nonlocal transport, the main implication of these results to hydrodynamic stability is a reduction in peak density and a corresponding increase in ablation velocity ( $V_a$ ), which is plotted in Fig. 54.2 as a function of time. The reduction in the Rayleigh-Taylor growth arising from the increased  $V_a$  is of obvious benefit to ICF.

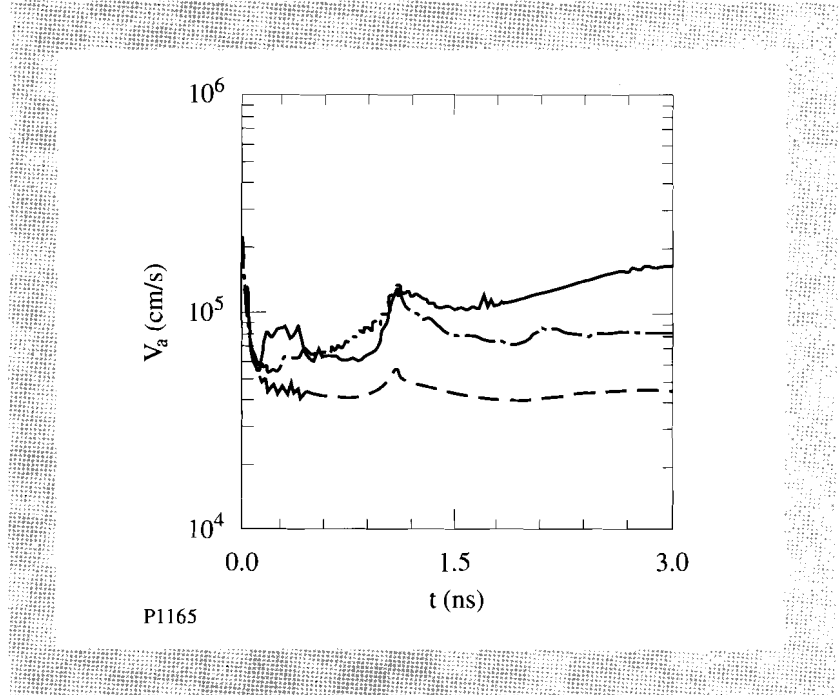


Fig. 54.2  
Plot of ablation velocity  $V_a$  in  $\text{cm s}^{-1}$  as a function of time (ns). Curves are identified as in Fig. 54.1.

However, the comparison previously made may be somewhat exaggerated because *SPARK* neglects radiation transport and ionization physics. To assess the relative importance of these effects, the *LILAC* hydrocode (at LLE) has been run under the same conditions (with no flux limit), but including a Thomas-Fermi equation of state, ionization from astrophysical tables, and radiation transport. The corresponding ablation-region profiles are plotted in Fig. 54.1, and  $V_a$  is plotted in Fig. 54.2 (dash-dotted curves). As observed, there is a significant impact from the additional physical effects included in *LILAC*. From this we may deduce that an accurate modeling of the experiments should include not only nonlocal heat transport, but also radiation and ionization effects.

## 2. Laser Filamentation in a 2-D Planar Plasma

Laser-filamentation experiments have been reported by Young,<sup>34</sup> where a 1.06- $\mu\text{m}$  laser beam with a 100-ps pulse length was intentionally modulated in space and made to interact with a preformed underdense CH plasma. These experiments have been successfully simulated using *SPARK*.<sup>4</sup> Recently, however, Rose and DuBois<sup>35</sup> claimed that Young's experiments should have been linearly stable to filamentation growth, by virtue of the finite  $f$ -number effects of the interaction beam. The motivation for the present simulations is, partly, to address this problem.

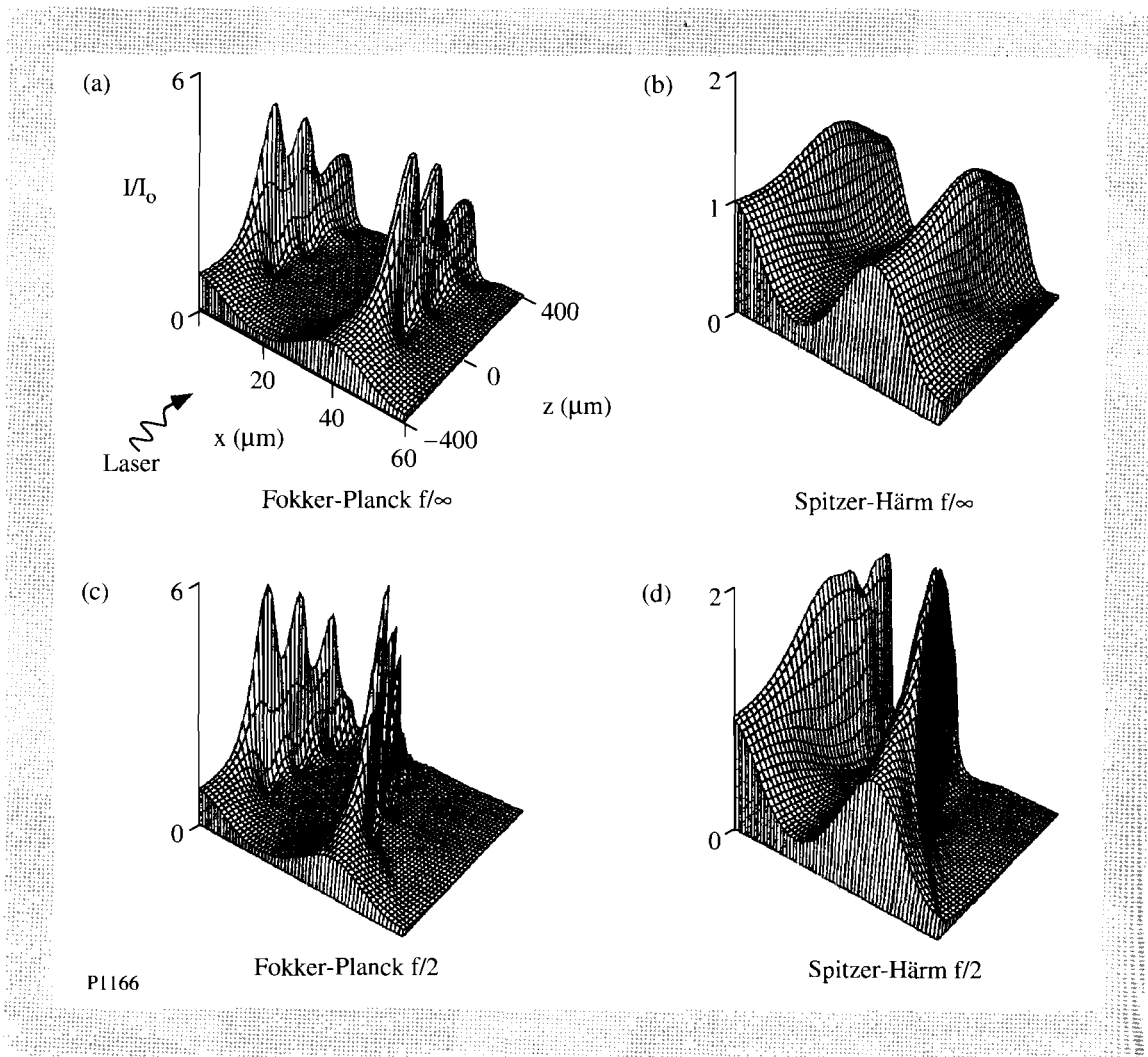
The simulation conditions have been described in detail by Epperlein and Short.<sup>4</sup> The plasma has an initial temperature of 0.8 keV, a uniform density in the  $x$ - $y$  plane,

and a parabolic density profile in the  $z$  direction, with a peak of one-quarter critical density at  $z=0$ . The interaction beam is spatially modulated in the  $x$  direction, with a wavelength of  $40\ \mu\text{m}$ , a peak intensity  $I_0$  of  $5 \times 10^{13}\ \text{W}/\text{cm}^2$ , and pulse width of  $100\ \text{ps}$ . Its propagation is calculated via the paraxial wave equation, and the convergence effect caused by the finite  $f$  number is modeled by using a spherical phase front with focus at  $x=0$ .<sup>36</sup> SPARK is run in 2-D planar geometry on a Eulerian mesh with  $\Delta x = 1\ \mu\text{m}$ ,  $\Delta z = 20\ \mu\text{m}$ ,  $\Delta v = 0.7v_p$ , and  $\Delta t = 0.01\ \text{ps}$ .

Figure 54.3 shows the surface plot of the normalized laser intensity  $I/I_0$  at the peak of the pulse with  $f/\infty$  and  $f/2$  optics and FP and SH thermal transport. The SPARK simulation took 80 min in CPU time on a CRAY Y-MP with an overall energy conservation error of 0.1%.

Fig. 54.3  
Surface plots of normalized laser intensity  $I/I_0$  with (a) FP transport and  $f/\infty$ , (b) SH transport and  $f/\infty$ , (c) FP transport and  $f/2$ , and (d) SH transport and  $f/2$ .

Comparison between FP and SH simulations confirms previous results that nonlocal heat transport enhances the laser filamentation rate.<sup>10,12</sup> More importantly, we find that the convergence effect caused by the  $f/2$  lens actually enhances the level of self-focusing, with the filaments following the ray trajectories, as observed experimentally.<sup>37</sup>



## Discussion and Conclusions

This article has shown that it is possible to write an efficient electron-FP, ion-fluid code to investigate 1-D and 2-D transport problems of interest to ICF. Briefly, to achieve this aim the FP equation is first simplified by means of a two-term angular expansion of the electron-distribution function, and the resultant equation is then solved via an ADI scheme. The *SPARK* code, which incorporates this approach, has been described in detail.

There are currently two main approximations in *SPARK*: it assumes a full ionization and it neglects radiation effects. Although these approximations may hold well in the hot, underdense corona of a laser-driven ICF pellet, the effects of ionization and radiation could be significant in the cold matter ahead of the main heat front. The implications of ionization effects, real equation of state, and radiation have already been demonstrated in Fig. 54.1, for the case of SH thermal transport. Within the FP formalism, the atomic physics would be incorporated in the form of additional collision operators that would model such processes as excitation, ionization, and recombination.

Another possible improvement to *SPARK* would be to introduce spatial mesh rezoning in 2-D transport simulations. This capability would allow for investigations of thermal smoothing and Rayleigh-Taylor instabilities.

## ACKNOWLEDGMENT

This work was supported by the U.S. Department of Energy Office of Inertial Confinement Fusion under Cooperative Agreement No. DE-FC03-92SF19460, the University of Rochester, and the New York State Energy Research and Development Authority. The support of DOE does not constitute an endorsement by DOE of the views expressed in this article.

## REFERENCES

1. A. R. Bell, R. G. Evans, and D. J. Nicholas, *Phys. Rev. Lett.* **46**, 243 (1981).
2. A. Nishiguchi *et al.*, *Phys. Fluids B* **4**, 417 (1992).
3. E. M. Epperlein and R. W. Short, *Phys. Fluids B* **3**, 3092 (1991).
4. E. M. Epperlein and R. W. Short, *Phys. Fluids B* **4**, 2211 (1992).
5. E. M. Epperlein, P. Amendt, L. Powers, and L. J. Suter, Laboratory for Laser Energetics Report No. 232 (1992).
6. S. I. Braginskii, *Reviews of Plasma Physics* (Consultants Bureau, New York, 1965), p. 205.
7. L. Spitzer, Jr. and R. Härm, *Phys. Rev.* **89**, 977 (1953).
8. R. C. Malone, R. L. McCrory, and R. L. Morse, *Phys. Rev. Lett.* **34**, 721 (1975).
9. A. R. Bell, *Phys. Fluids* **26**, 279 (1983).
10. E. M. Epperlein, *Phys. Rev. Lett.* **65**, 2145 (1990).
11. E. M. Epperlein, in *Research Trends in Physics: Nonlinear and Relativistic Effects in Plasmas*, edited by V. Stefan (American Institute of Physics, New York, 1991), p. 43.

12. E. M. Epperlein, Phys. Fluids B **3**, 3082 (1991).
13. R. W. Short and E. M. Epperlein, Phys. Rev. Lett. **68**, 3307 (1992).
14. E. M. Epperlein and R. W. Short, Phys. Fluids B **4**, 4190 (1992).
15. H. A. Rose and D. F. DuBois, Phys. Fluids B **4**, 1394 (1992).
16. M. N. Rosenbluth, W. M. MacDonald, and D. L. Judd, Phys. Rev. **107**, 1 (1957).
17. E. M. Epperlein, G. J. Rickard, and A. R. Bell, Phys. Rev. Lett. **61**, 2453 (1988).
18. E. M. Epperlein, G. J. Rickard, and A. R. Bell, Comput. Phys. Commun. **52**, 7 (1988).
19. A. B. Langdon, Phys. Rev. Lett. **44**, 575 (1980).
20. J. R. Sanmartin *et al.*, Phys. Fluids B **4**, 3579 (1992).
21. R. J. Mason, J. Comput. Phys. **41**, 233 (1981).
22. R. D. Richtmyer and K. W. Morton, *Difference Methods of Initial-Value Problems* (Wiley, New York, 1967), p. 313.
23. J. Douglas, Jr., Numer. Math. **4**, 41 (1962).
24. J. Douglas, Jr. and J. E. Gunn, Numer. Math. **6**, 428 (1964).
25. W. R. Briley and H. McDonald, J. Comput. Phys. **34**, 54 (1980).
26. R. J. Wright, J. Phys. D: Appl. Phys. **14**, 805 (1981).
27. G. J. Pert, J. Comput. Phys. **49**, 1 (1983).
28. J. S. Chang and G. Cooper, J. Comput. Phys. **6**, 1 (1970).
29. A. B. Langdon, in *CECAM Report of Workshop on "The Flux Limiter and Heat Flow Instabilities in Laser-Fusion Plasmas"* (Université Paris Sud, France, 1981), p. 69.
30. J. P. Matte, T. W. Johnston, J. Delettrez, and R. L. McCrory, Phys. Rev. Lett. **53**, 1461 (1984).
31. T. H. Kho and M. G. Haines, Phys. Fluids **29**, 2665 (1986).
32. R. P. J. Town and A. R. Bell, in *CECAM Report of Workshop on "Laser-Plasmas Interactions"* (Université Paris Sud, France, 1991), p. 36.
33. S. G. Glendenning, S. V. Weber, P. Bell, L. B. DaSilva, S. N. Dixit, M. A. Henesian, D. R. Kania, J. D. Kelkenny, H. T. Powell, R. J. Wallace, P. J. Wegner, J. P. Knauer, and C. P. Verdon, Phys. Rev. Lett. **69**, 1201 (1992).
34. P. E. Young, Phys. Fluids B **3**, 2331 (1991).
35. H. A. Rose and D. F. DuBois, Phys. Fluids B **4**, 252 (1992).
36. J. A. Fleck, Jr., J. Comput. Phys. **16**, 324 (1974).
37. P. E. Young *et al.*, Phys. Rev. Lett. **61**, 2336 (1990).